NUCLEAR g-FACTORS IN ^{55}Fe

NUCLEAR g-FACTORS IN IRON 55

FROM

PERTURBED ANGULAR CORRELATION STUDIES

By

PETER GEORGE KERR, B.Sc.

A Thesis

Submitted to the Faculty of Graduate Studies

in Partial Fulfilment of the Requirements

for the Degree

Master of Science

McMaster University

August 1973

MASTER OF SCIENCE (1973) McMASTER UNIVERSITY
(Physics) Hamilton, Ontario

TITLE: Nuclear g-Factors in Iron 55 from Perturbed Angular Correlation Studies.

AUTHOR: Peter George Kerr, B.Sc. (Liverpool University)

SUPERVISOR: Dr. J. A. Cameron

NUMBER OF PAGES: vii, 53

SCOPE AND CONTENTS:

The (α,n) reaction on natural chromium has been used to study levels in ^{55}Fe up to 2.5 MeV excitation. Intensities and angular distributions of the decay gamma rays were measured, yielding branching and $\frac{E_2}{M_1}$ mixing ratios. In a magnetized target of the alloy $Cr_{20}Fe_{80}$, the rotation of the angular distributions was observed. Using recently determined lifetimes and the average internal field of 277 kOe measured in the target material by Mössbauer absorption, the following g-factors are obtained:-

931 keV , $5/2^-$ -: +1.2 ± 0.5

1316 keV , $7/2^-$ -: +0.5 ± 0.5

1408 keV , $7/2^-$ -: -0.77 ± 0.16

ACKNOWLEDGEMENTS

Particular thanks must go to my supervisor, Dr. J. A. Cameron, for the initiation of this project and for constant help and interest during its progress.

During the course of the work, invaluable assistance was freely given by Alan Gibb, who taught me the experimental techniques involved, Stephen Barrett, who offered much of his time to helping with the experiments and Tom Dececchi, who helped during his summer with the group.

I would like to thank also the staff of the McMaster University FN Tandem Accelerator for continual assistance on technical matters.

Apologies go to my patient wife, Elizabeth, for the irregular hours involved in carrying out accelerator experiments.

This research was supported by grants to the group by the National Research Council and financial assistance to the author from McMaster University and the Government of the Province of Ontario.

This thesis is dedicated to the following:-

C,C,D,D,D,D,E,J,J,M,M,W,Y

,with special thanks to

"THE LITTLE RED FIRE ENGINE".

P.G.K. (July,1973)

TABLE OF CONTENTS

LIST OF ILLUSTRATIONS

LIST OF ILLUSTRATIONS (CONTINUED)

LIST OF TABLES

CHAPTER I

INTRODUCTION

If a nucleus interacts with a static magnetic field H, a classical precession of the nuclear spin axis about the field can be said to occur. The frequency of the rotation is called the Larmor precession frequency and is given by the equation

$$\omega = \frac{g\mu_N H}{\hbar}$$

where μ_N is the nuclear magneton and g is the nuclear g-factor. In principle then if this rotation can be measured in a known field, one has a method of measurement of magnetic moments of nuclear states.

If one observes the nucleus in the intermediate state of a cascade for which there is an anisotropic angular correlation, this correlation will be perturbed, should the nuclear precession be large enough. The size of the measured perturbation will depend critically on the magnetic field applied and the lifetime of the intermediate state. Difficulty arises in observing an angular correlation if the lifetime is too long. The angular correlation will be removed if the fields acting on the nucleus are large enough to cause a considerable amount of mixing of the magnetic substates of the intermediate level.

Early experiments utilized the fields produced by an electromagnet (Aeppli et al. 1951, Frauenfelder et al. 1954) but these are, of course, limited by practical considerations. Nowadays most experiments utilize

the hyperfine fields on the nucleus due to its orbital electrons, which are known to be greater than the fields which are produced by conventional electromagnets.

To be of use, the fields need to have a known magnitude and direction. This is achieved most easily of course in ferromagnetic samples. At temperatures well below the Curie point the electronic magnetic moments of a ferromagnet are essentially all lined up when regarded on a microscopic scale. Yet, looking at a specimen as a whole, the magnetic moment may be very much less than the saturation moment, and the application of an external magnetic field may be required to saturate the specimen. It is thought that actual specimens are composed of a number of small regions called domains, within each of which the local magnetization is saturated. The electrons inside a domain of the ferromagnet are polarized in a definite direction and the domains can easily be aligned along an external applied field, provided that field produces magnetic saturation in the sample. Many techniques are available to measure these hyperfine fields. In this particular work the technique of Mössbauer absorption was employed.

The work to be described in this thesis was undertaken primarily to determine static magnetic dipole moments of the lower lying states of ^{55}Fe. As a by-product, branching and multipole mixing ratios for several transitions have been redetermined.

^{55}Fe is an odd neutron nucleus with 29 neutrons and lies just above ^{54}Fe in the periodic table, the latter having a closed even-even core. Such nuclei may generally be described well by coupling the last particle

(or hole) to the even-even core, whose excitations are treated in the shell model as two-particle states or in the collective model as vibrations. Nuclei with 29 neutrons have been treated in this way in a number of recent papers (eg. Carola and Ohnuma, 1971, Csűrös et al. 1971, and earlier work cited by these authors).

Previous experimental work on ^{55}Fe has been largely with the (d,p), (p,d), (n,γ) and (p,nγ) reactions. Extensive work of this kind by Pilt et al. (1970) and also Robertson et al. (1970,1972) has provided much information about the electromagnetic properties of the ^{55}Fe levels. In general good agreement is obtained for energies, electromagnetic transition rates and particle transfer cross-sections between the experiments and calculations in which the 29th neutron, in the p 3/2, p 1/2 and f 5/2 subshells is coupled to the ^{54}Fe core. Additional high-spin states attributable to the generation of neutron hole states appear at low excitation energies. In ^{55}Fe the levels at 1408 and 2301 keV are thought to be of this nature. In general the hole states have the characteristic of not being strongly mixed with the particle excitations. This is apparent from the particle transfer work and from gamma transition strengths.

The experiment used in this study was ^{52}Cr (α,n) ^{55}Fe. It is known that there is a high degree of alignment possible in (α,n) reactions on spin-zero targets, even well above the reaction threshold and therefore this reaction is a good choice. In addition, the magnetic moment study was aided by the comparatively high solubility of chromium in iron. Thus it was possible to use the large internal field in a ferromagnetic alloy

target containing an appreciable proportion of the target isotope. Since the final nucleus was one of iron, a simple and direct calibration of the internal field was made using the Mössbauer effect of ^{57}Fe naturally occurring in the target.

CHAPTER II

ANGULAR CORRELATION THEORY

Several authors have written substantial articles on the theory of perturbed angular correlations (Frauenfelder et al. 1965, Ferguson, 1965) and for more detailed description than will be given here, the reader is referred to these.

Consider first unperturbed angular correlations of gamma rays emitted from aligned states formed by nuclear reactions. The work in this thesis involved the (α,n) reaction and it is well known that in such reactions a high degree of alignment exists, and gamma rays therefore show angular distributions which depend strongly on the multipolarities and spin sequences present.

A particularly full treatment of the angular distribtuion of γ-rays emitted from aligned states may be found in the review article of Rose and Brink (1967). A summary of their theory is given below. Consider the reaction A (a,b)B* with neither the target nucleus A nor the beam of particles a being polarized. Let the axis of quantization be defined along the direction of the incoming beam. Then if the residual nucleus B*, in an excited state $|J,m\rangle$ with definite parity can be said to be aligned the population parameters $P(m_1)$ for the ensemble must satisfy the relations

$$P(m_1) = P(-m_1)$$

$$\text{and } P(m_1) \neq \frac{1}{2J_1 + 1}$$

J_1 denoting the initial nuclear spin.

P(m) may be defined in the following way. It is the probability that the m substate is populated and the following condition must hold

$$\sum_{m=-J}^{J} P(m) = 1$$

This leads to the idea of an isotropic state for if all the $P(m) = \frac{1}{2J + 1}$ then there is no preferred axis and the decay of the nucleus B* will be isotropic.

Now consider the state $|J_1 m_1>$ decaying to a state $|J_2 m_2>$, letting q define the circular polarization ($q = \pm 1$). The probability amplitude for such a transition may now be written

$$A^{q}_{m_1 m_2}(\underset{\sim}{k}) = -\sqrt{\frac{k}{\hbar}} \sum_{LM\pi} q^{\pi} <J_1 m_1 | T^{L\pi}_{M} | J_2 m_2> D^{L}_{Mq}(R)$$

Here $D^{L}_{mq}(R)$ is the rotation matrix which takes the beam axis z into the direction $\underset{\sim}{k}$ and $T^{L\pi}_{M}$ is the appropriate transition matrix.

Now if the orientation of the spin J_2 of the final state is not observed, then the probability of transition from the state $|J_1 m_1>$ to any substate of J_2 by the emission of a photon is

$$\sum_{m_2} |A^{q}_{m_1 m_2}(\underset{\sim}{k})|^2$$

This now allows us to write the transition probability as the sum of the above weighted according to the relative population of each initial substate $|J_1 m_1>$

ie

$$\sum_{m_1} P(m_1) \sum_{m_2} \left| A^q_{m_1 m_2}(k) \right|^2$$

This expression may now be evaluated using the Racah algebra giving for the angular distribution of circularly polarized gamma rays.

$$W(\theta, J_1 \to J_2; q) = \frac{k}{\hbar} \sum_{KLL'} \rho_K(J_1) P_k(\cos\theta)$$

$$\times (-1)^{q+J_1-J_2+L'-L-K} \sqrt{2J_1+1} \; \langle L\, L'\; q-q \mid K0 \rangle$$

$$\times W(J_1 J_1 LL'; KJ_2)\; q^{\pi+\pi'} \langle J_1 || T^{L\pi} || J_2 \rangle \langle J_1 || T^{L'\pi'} || J_2 \rangle$$

where ρ_K is given by

$$\rho_K(J_1) = \sum_{m_1} P(m_1)(-1)^{J_1-m_1} \sqrt{2J_1+1} \; \langle J_1 m_1 \; J_1 - m_1 | K0 \rangle$$

Now in this summation, assuming $L' \geq L$, K is limited to the even integer $\leq \min(2L', 2J_1)$ because of the Racah coefficient and the assumption that

$$P(m_1) = P(-m_1)$$

Now generally it is sufficient to consider only the lowest two multipole orders L and L' in the analysis. The multipole mixing ratio δ may then be defined as

$$\delta = \frac{\langle J_1 || T^{L'\pi'} || J_2 \rangle}{\langle J_1 || T^{L\pi} || J_2 \rangle} \quad \frac{2L'+1}{2L+1} \quad ; \; L' = L+1$$

If polarization is not observed, then the incoherent sum over the circular polarization index q is taken, and the angular distribution may then be written,

$$W(\theta) = \sum_K A_K P_K(\cos\theta)$$

where

$$A_K = \rho_K(J_1) \frac{R_K(LLJ_1J_2) + 2\delta R_K(LL' J_1J_2) + \delta^2 R_K(L' L' J_1J_2)}{1+\delta^2}$$

and

$$R_K(LL' J_1J_2) = (-1)^{1+J_1-J_2+L'-L-K} \sqrt{(2J_1+1)(2L+1)(2L'+1)}$$

$$\cdot \langle L1L' -1 | K0 \rangle W(J_1J_1LL' ; KJ_2)$$

In this expression, $\rho_K(J_1)$ contains all the information on the alignment of the initial state $|J_1m_1\rangle$. The R_K terms depend specifically on the geometry of the $J_1 \rightarrow J_2$ cascade and they are tabulated for spins ≤ 10 by Rose and Brink. Tabulations have also been made by Yamazaki (1967) for even greater spins. The internal nuclear properties affect the distribution through the mixing ratio δ.

Now since A_o is proportional to the intensity of the γ-ray, it is usual to quote the normalized angular distribution coefficients

$$a_2 = A_2 | A_o$$

and $$a_4 = A_4 | A_o$$

The angular distribution may also be written in the form,

$$W(\theta) = \sum_K b_K \cos K\theta$$

where the following simple algebraic relations hold between the a_K's and b_K's

$$b_2 = \frac{\frac{3}{4} a_2 + \frac{5}{16} a_4}{1 + \frac{1}{4} a_2 + \frac{9}{64} a_4}$$

and $$b_4 = \frac{\frac{35}{64} a_4}{1 + \frac{1}{4} a_2 + \frac{9}{64} a_4}$$

It is clear that a_2 and a_4 are fixed by a large number of nuclear parameters (especially in the case of mixed multipoles) including nuclear spins, multipole orders and mixing ratios δ, and in general one will need additional nuclear data to determine the mixing ratios. The coefficients will be highly sensitive to the reaction mechanism and this is given essentially by $\rho_K(J_1)$, the statistical tensor describing the relative substate populations of the initial state of the transition. In the present work angular distributions were analyzed without recourse to the use of mechanism - dependent statistical tensors. Whenever possible, the mixed transitions were compared directly with pure E_2 decays from the same initial state.

CHAPTER III

PERTURBED ANGULAR CORRELATION THEORY

If during a nuclear reaction, a magnetic field is applied while the nuclei are in the excited state, then their magnetic moments will execute Larmor precession about the field direction. This will alter the nuclear orientation, and a change in the relative magnetic substate populations will occur. This results in a modification of the angular distribution of the de-excitation gamma rays. Detection of a gamma-ray, which must have an angular momentum component of ±1 in its direction of travel, selects a particular ensemble of excited nuclei all of whose members have an angular momentum projection in the direction perpendicular to the plane of detection. If a static magnetic field is applied perpendicular to this plane, this ensemble precesses about the field direction, but the nuclei do not change their angular momentum projection along the field direction. Detailed analysis shows that the entire gamma ray angular distribution rotates through an angle ωt where ω is the Larmor precession frequency and t is the time during which the magnetic field acts.

The introduction of an unequal population of the m states in the intermediate state by the detection of the first radiation of a cascade, with wave vector $\underset{\sim}{k}_1$ in a given direction, may conveniently be described by the density matrix $\langle m|\rho(\underset{\sim}{k}_1,0)|m'\rangle$ given by,

$$\langle m|\rho(\underset{\sim}{k}_1,0)|m'\rangle = (4\pi)^{\frac{1}{2}} \sum_k (-1)^m A_k(1) \begin{pmatrix} I & I & k \\ m' & -m & \mu \end{pmatrix} Y_{k\mu}^*(\underset{\sim}{k}_1)$$

Here 0 denotes zero time after the alignment of the state. $\begin{pmatrix} I & I & k \\ m' & & m\mu \end{pmatrix}$ is a Clebsh-Gordan coefficient and $Y_{k\mu}^{*}(k_1)$ is a spherical harmonic expressing the angular dependence.

For a second transition we have

$$\langle m'|\rho(\underset{\sim}{k}_2)|m\rangle=(4\pi)^{\frac{1}{2}}\sum_{k'}(-1)^{m}A_{k'}(2)\begin{pmatrix} I & I & k' \\ m' & -m & \mu \end{pmatrix} Y^{*}_{k\mu}(\underset{\sim}{k}_2)$$

The unperturbed angular correlation may thus be written as the trace of the product of these density matrices.

$$W(\theta,0) = W(\underset{\sim}{k}_1,\underset{\sim}{k}_2,0)$$

$$= \mathrm{Tr}\ \{\rho(\underset{\sim}{k}_1,0),\rho(\underset{\sim}{k}_2)\}$$

$$= \sum_{mm'}\langle m|\rho(\underset{\sim}{k}_1,0)\ |m'\rangle\langle m'|\rho(\underset{\sim}{k}_2)|m\rangle$$

Now on application of the static magnetic field, interactions will occur in the intermediate state, and the density matrix will now become time dependent

$$\rho(\underset{\sim}{k}_1,0) \rightarrow \rho(\underset{\sim}{k}_1,t)$$

We then have

$$W(\theta,t) = W(\underset{\sim}{k}_1\underset{\sim}{k}_2,t) = \sum_{mm'}\langle m|\rho(\underset{\sim}{k}_1,t)|m'\rangle\langle m'|\rho(\underset{\sim}{k}_2)|m\rangle$$

t being the delay introduced in the angular correlation experiment. The time dependence of the density matrix is given by the Heisenberg equation of motion,

$$\frac{\partial\rho}{\partial t} = \frac{-i}{\hbar}\left[H,\rho\right]$$

This becomes for a static interaction

$$\rho(\underset{\sim}{k},t) = \Lambda(t)\ \rho(\underset{\sim}{k},0)\ \Lambda^{-1}(t)$$

$\Lambda(t)$ being the evolution operator given by

$$\Lambda(t) = \exp(-\frac{i}{\hbar} H \cdot t)$$

Now if the expressions for $\rho(k_1,t)$ and $\rho(k_2)$ are substituted into the expression for $W(\theta,t)$ and the result compared with the expression obtained by substitution into $W(\theta,0)$, a general form for the attenuation coefficients, $G_k(t)$, is obtained

$$G_k(t) = \sum_{\substack{mm' \\ m''m'''}} \{(\text{geometric factors}) \; X\langle m|\Lambda(t)|m''\rangle\langle m'|\Lambda(t)|m'''^*\rangle\}$$

and finally we arrive at the most general form of the perturbed angular correlation

$$W(\underset{\sim}{k}_1,\underset{\sim}{k}_2,t) = 4\pi \sum_{\substack{kk' \\ \mu\mu'}} \frac{A_k(1)\; A_k(2)}{(2_k+1)(2_{k'}+1)} \quad G_{kk'}^{\mu\mu'}(t)\; Y_{k\mu}^*(\underset{\sim}{k}_1) X\; Y_{k'\mu'}(\underset{\sim}{k}_2)$$

In the present context, the most useful case to discuss is that of a static magnetic field which is perpendicular to the correlation plane. If $G_k(t)$ is evaluated, the classical result that the angular correlation precesses with the Larmor frequency ω_L about the direction of the field is obtained.

We then have,

$$W(\theta,t) = \sum_k A_k P_k [\cos\; (\theta-\omega_L t)]$$

or equivalently,

$$W(\theta,t) = \sum_k b_k \cos\; k\; (\theta-\omega_L t)$$

Should one be dealing with short nuclear lifetimes, a time integral angular correlation must be measured. eg. For the case of a magnetic field H perpendicular to the reaction plane we have,

$$W(\theta,H) = \frac{1}{\tau}\int_0^\infty W(\theta,t)\, e^{-t/\tau} dt$$

$$= \sum_k \frac{b_k(\cos k\theta + k\omega\tau \sin\theta)}{1+(k\omega\tau)^2}$$

with $\omega\tau$ the mean rotation angle being given by

$$\omega\tau = \frac{g\mu_N H\tau}{\hbar}$$

In practice what is measured is the counting rate $W(\theta,H)$ produced by the gamma rays at $\theta = 135^\circ$ and 225° for the two possible directions of the external magnetic field, up and down (+H and -H), the results being quoted in the form,

$$Q^2 = \frac{W\,(135^\circ, +H)\,.W\,(225^\circ, -H)}{W\,(135^\circ, -H)\,.W\,(225^\circ, +H)}$$

The reason for choosing the angles 135° and 225° is that these are the positions of the maximum slope of the angular correlation function when $b_4 << b_2$.

The average rotation angle is related to Q by

$$\frac{Q-1}{Q+1} = \frac{2b_2\ \omega\tau\,|\left[1+(2\omega\tau)^2\right]}{1-b_4\,|\left[1+(4\omega\tau)^2\right]}$$

and may thus be measured.

CHAPTER IV

HYPERFINE FIELDS AND THEIR MEASUREMENT USING THE MÖSSBAUER ABSORPTION TECHNIQUE

In present day perturbed angular correlation work it is usual to use the large internal hyperfine field acting on an impurity in a host ferromagnetic lattice as the perturbing field, rather than the smaller fields which can be produced using conventional electromagnets. The usual choice of ferromagnetic host is iron, cobalt or nickel since these are all ferromagnetic at room temperature and many nuclei of interest are soluble in one or more of them. In general, for low concentration alloys, the hyperfine field does not depend greatly on the amount of impurity present but this may not be the case for higher concentration alloys.

Several authors have discussed the theory of hyperfine fields in solids (eg. Marshall (1958), Watson and Freeman (1961), Shirley and Westenbarger (1965)) and the reader is referred to these review articles for discussions of their origin. The two major contributions to the hyperfine field are conduction-electron polarization and core-polarization. These are exchange polarizations of the conduction or core s-electrons of a metallic impurity inside the host lattice, creating a hyperfine field at the impurity nucleus by a Fermi contact interaction. In the case of iron and 3d magnetic elements, core polarization is thought to dominate.

Several techniques have been used to measure many of the hyperfine fields and among the most useful of these techniques is the recoilless

emission and absorption of gamma rays - the Mössbauer effect - so named after its discovery in 1958 by R. L. Mössbauer. He showed that nuclei embedded in solids can emit and absorb low-energy gamma rays with all the recoil momentum being transferred to the lattice in the process. A brief summary of the underlying theory follows.

Consider an excited state of a free atom or nucleus (mass M) which decays to the ground state, emitting a photon as it does. The photon will be emitted with energy $P = \hbar\underset{\sim}{k}$ and the nucleus must therefore recoil with momentum $P = -\hbar\underset{\sim}{k}$. It will therefore have a recoil energy given by

$$E \text{ recoil} = \frac{\hbar^2 k^2}{2M} = \frac{E\gamma^2}{2Mc^2}$$

$E\gamma$ is the gamma-ray energy.

Energy must be conserved and so we may write,

$E\gamma = E_0 - E_R$, where E_0 is the nuclear excitation energy.

Now $E_R << E\gamma$ in general and hence we may write,

$$E_R \approx \frac{E_0^2}{2Mc^2}$$

Therefore we have

$$E\gamma = E_0 - E_R = E_0 - \frac{E_0^2}{2Mc^2}$$

Therefore the gamma ray imparts an energy E_R to the emitting nucleus. If the photon had been absorbed it would have had an energy $E_0 + E_R$. Clearly then there is an energy difference between the emitted and absorbed photons of $2E_R$. If $2E_R$ is less than the width Γ of the excited nuclear state resonance absorption can occur ie. there must be an

appreciable overlap of the emission and absorption lines ($\Gamma/2E_R \gg 1$). This is seen in figure 1(a). Here Γ, the natural line width of the emitted photon is given by the Heisenberg uncertainty relation $\Gamma\tau = \hbar$, where τ is the lifetime of the excited state. The Mössbauer effect can be seen by an increase in scattered radiation or a decrease in the transmitted intensity. The usual method used is to Doppler shift a source relative to an absorber - usually by producing an energy shift greater than the natural line width by moving the source with a velocity with respect to the absorber. Experimentally, the source is attached to a velocity device and the absorber and a counter are used to measure the reduced intensity. The intensity transmitted is then plotted as a function of velocity and in general at large velocities no resonance absorption will occur.

Perhaps of all nuclei the ^{57}Fe nucleus has proved the most useful in Mössbauer studies - particularly in the field of magnetism. The decay scheme of ^{57}Fe is shown in figure 1(b). The 14.4 keV transition from the 3/2 - → 1/2 - state is the one used in many Mössbauer experiments. The following data on this state at 14.4 keV is available.

Half-life $\tau = 1.4 \times 10^{-7}$ sec.

Natural line width $\Gamma = 4.7 \times 10^{-9}$ eV

Doppler velocity corresponding $v_r = \frac{\Gamma}{E_0} c$

$= 0.095$ cm/sec

Debye temperature in iron, $\theta_D \approx 420^\circ$ to $470^\circ K$

Recoilless fraction (with $\theta_D = 420^\circ K$,)

Figure 1

(a) Mössbauer effect: Overlap of emission and absorption lines showing the condition for resonance absorption

(b) Decay scheme of ^{57}Fe

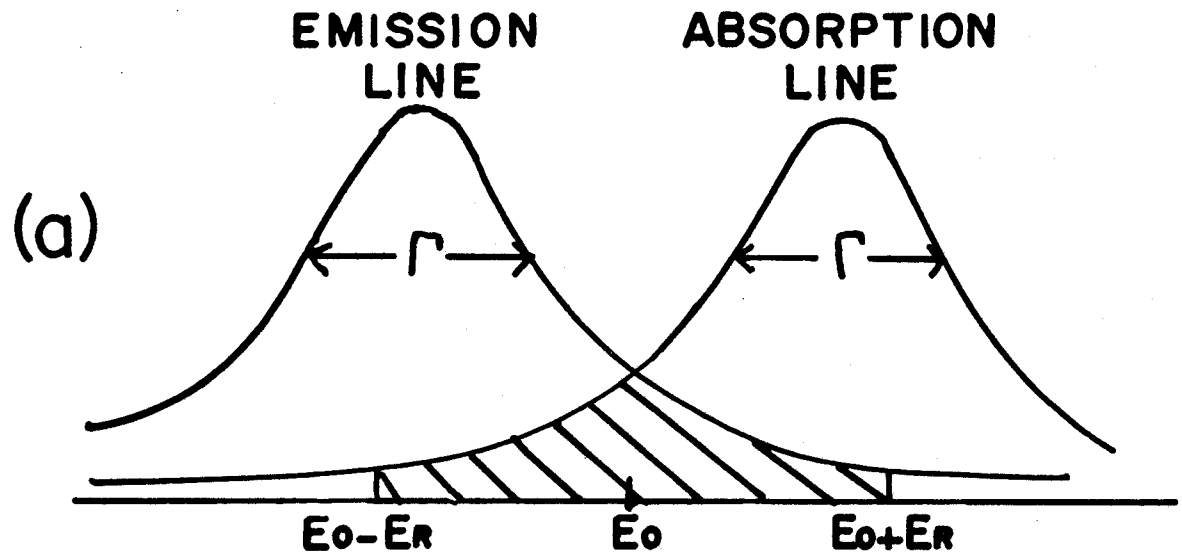
(a)
EMISSION LINE
ABSORPTION LINE
Γ
Γ
E0-ER
E0
E0+ER

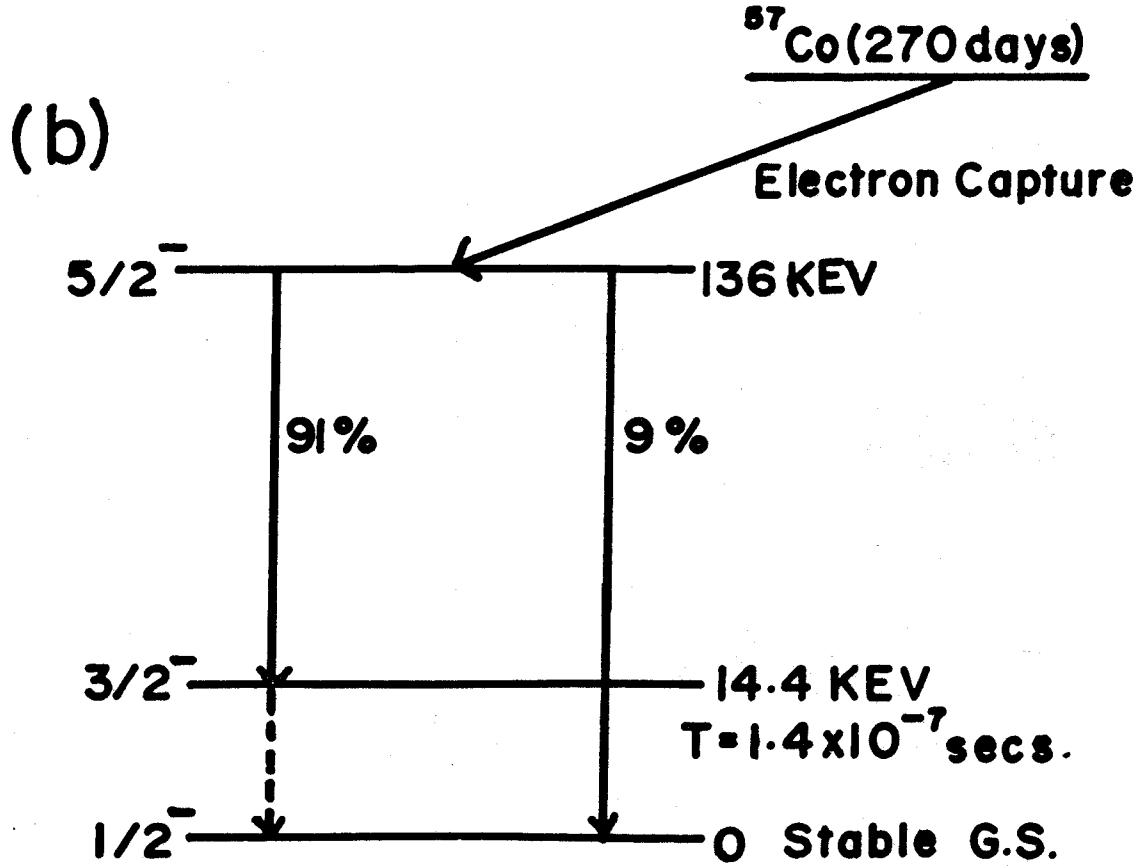
(b)
57Co(270 days)
Electron Capture
5/2⁻
136 KEV
91%
9%
3/2⁻
14.4 KEV
T=1.4x10⁻⁷ secs.
1/2⁻
0 Stable G.S.

$f(0^{o}K) = 0.92$; $f(300^{o}K) = 0.79$

The latter implies that in general low temperature equipment is not required.

If no magnetic or electric fields are present, degeneracy will mean that the spectrum observed will be merely a single transition line. If a field H_{eff} is now applied, interaction occurs with the magnetic moments of the ground state μ_o and excited state μ_1 causing a Zeeman splitting of the nuclear levels - see Fig. 2 . Six possible transitions governed by the selection rules for dipole radiation will occur and the resultant spectrum will be as in figure 10(b) in Chapter VII of this thesis.

Many experiments on both dilute and non-dilute alloys of iron have been carried out and the main result has been that there appears to be a linear dependence between the field measured and the electron spin density. It is characteristic of the experiments that a line broadening occurs in the spectrum. This naturally leads to the belief that the observed field is actually an average over a range of fields which are present in the alloy. Attempts have been made to reconstruct the experimental curves by assuming an effective magnetic field depending on the number of iron nearest neighbours and weighting these according to the statistics of the alloy. Such reconstructions have proved successful in many cases.

For dilute iron alloys (ie. dilute solutions of impurity elements in iron) the distinct hyperfine fields associated with the many local environments have been resolved experimentally. It appears that nearest neighbours alone determine the field, the field for iron atoms with all iron nearest neighbours being the same as that in metallic iron but each

Figure 2

Hyperfine splittings of nuclear levels in ^{57}Fe on application of a magnetic field

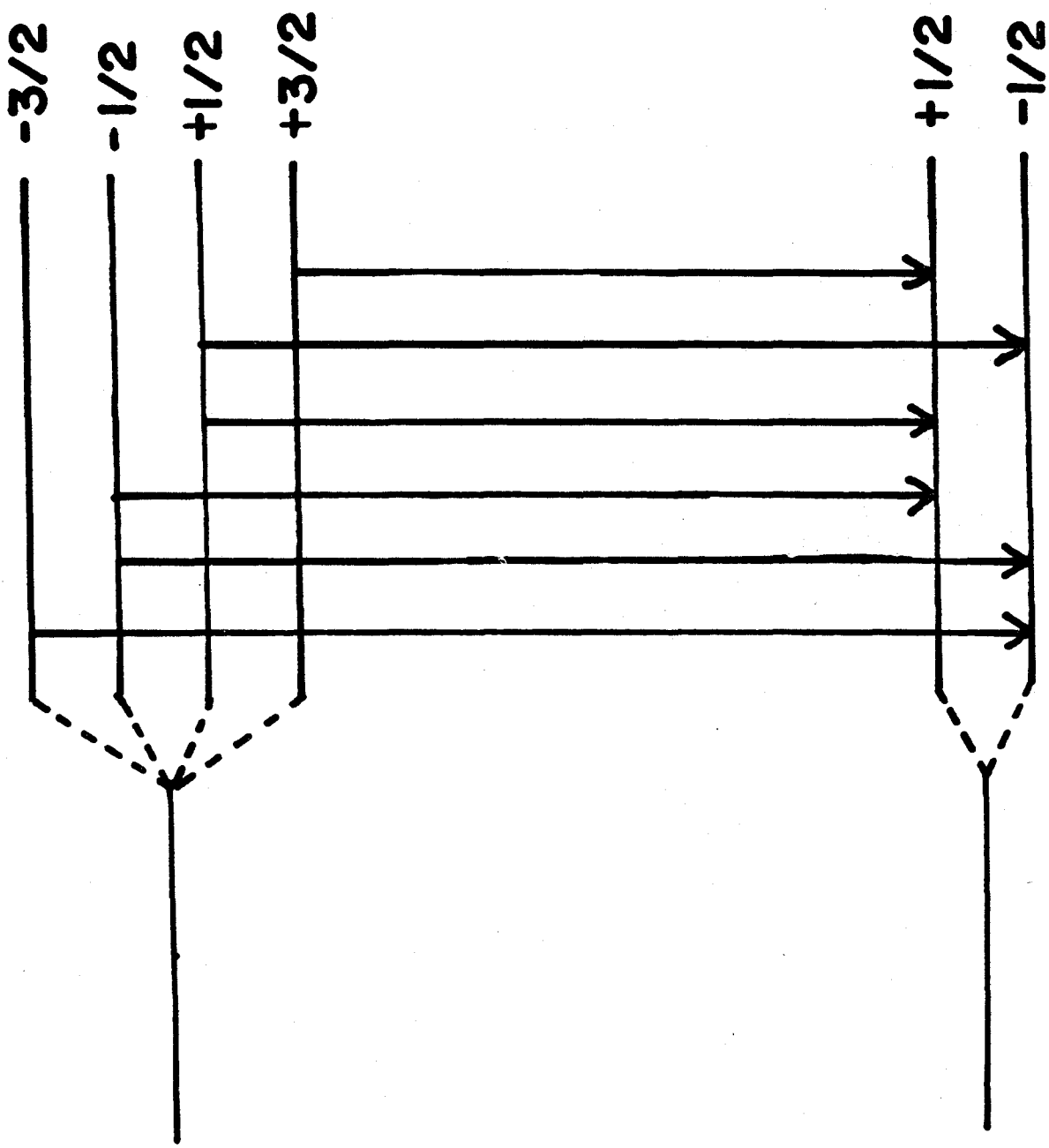
-3/2
-1/2
+1/2
+3/2
+1/2
-1/2

impurity neighbour reducing the field by a fixed amount. An important finding has been that all near neighbour impurities except Co and Ni reduce the hyperfine field by approximately 8%. According to magnetization measurements, the moment of these atoms changes little indicating that the ratio of hyperfine field to moment is seriously perturbed by a near neighbour impurity.

Consider the introduction of a single foreign atom at the origin into a body centred cubic lattice. The solute atom will be in a position of cubic symmetry but the host atoms will not. There is degeneracy however, in that atoms in a given neighbour shell are in equivalent positions. If a magnetization axis is added this degeneracy will be lifted, eg. for the case of the axis being in the [111] direction first neighbours are split into two groups - two atoms lying on the axis and the other six atom off the axis. However, six atoms in the second neighbour shell are in equivalent positions. Should the magnetization axis be in the [001] direction the eight first neighbour atoms will now be in equivalent positions, with the second neighbour ones consisting of two atoms on the axis and four atoms off the axis. This type of analysis may be extrapolated to discuss non-dilute alloys.

For an iron atom with N_n impurities as nearest neighbours and N_{nn} next - nearest impurity neighbours the hyperfine field may be written in the form

$$H(N_n, N_{nn}) = H'\{1 + C_n N_n + C_{nn} N_{nn} \ldots + \text{etc.}\}$$

and H', C_n and C_{nn} must be determined experimentally. If the crystal is of a given impurity concentration and if it is assumed that the impurities

have gone into the crystal in a statistically independent way, the number of Fe atoms with particular values of N_n and N_{nn} may be obtained. For low concentration alloys of chromium (as well as Si,V, Mn and Ru) C_n and C_{nn} seem to be well fixed constants. In fact $C_n \sim -0.075$ and $C_{nn} \sim -0.006$, the negative sign indicating the known reduction of the hyperfine field with increasing numbers of impurity neighbours.

CHAPTER V

ANGULAR DISTRIBUTION MEASUREMENTS IN ^{55}Fe

Angular distribution measurements were carried out using the $^{52}Cr(\alpha,n)^{55}Fe$ reaction, by bombarding a target of pure chromium with a beam of 7MeV alpha particles from the McMaster University FN tandem accelerator facility. The target chamber used is shown schematically in figure 6, Chapter VI and is described more fully elsewhere (A. Gibb, Thesis 1973). Ge(Li) detectors were used of 50 cc and 12 cc volume. Since the level in ^{55}Fe at 411 KeV has spin - 1/2 its decay gamma ray could be used as a normalization peak and hence both counters were moved in the backward quadrants 90^{o} to 270^{o}. Care was taken to ensure that the detectors remained the same distance from the target at the different angle settings to alleviate the necessity of making any solid angle corrections to the data. The spectra were collected on a PDP-9 on-line computer and were analyzed off-line on a CDC-6400 computer. A typical gamma-ray spectrum obtained is shown in figure 3.

The angular distributions were fitted to a form

$$W(\theta) = \sum_{k\ (\text{even})} A_k' P_k (\cos\theta)$$

and as stated earlier the coefficients A_k depend not only on spins of levels and the transition multipole order but also on the reaction mechanism. This latter dependence may be separated using the Racah algebra associated with the statistical tensor $\rho_k(J_1)$ describing the

Figure 3

Ge(Li) gamma-ray spectrum for a pure chromium target bombarded with 7MeV α particles

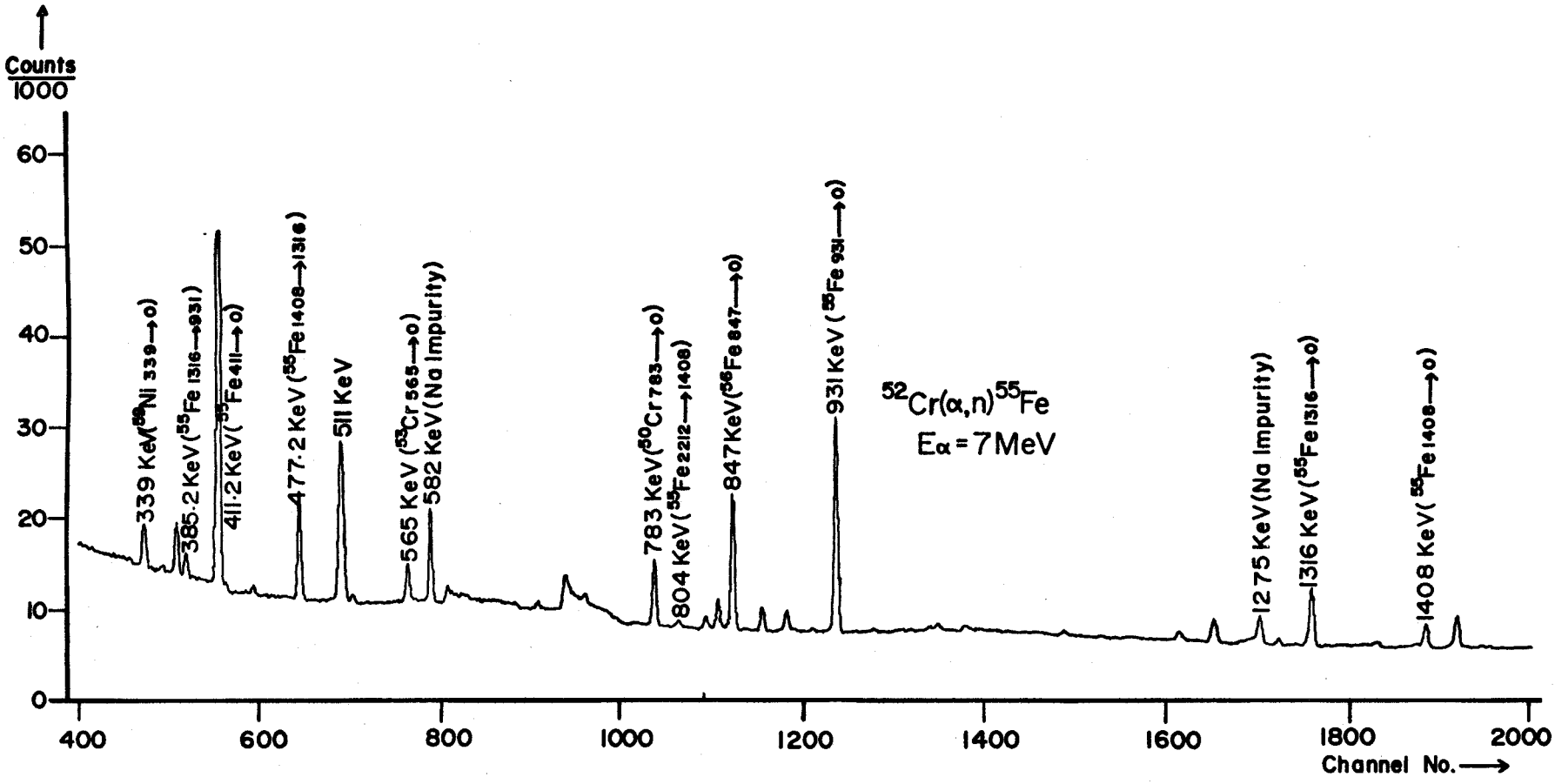
Counts
1000
60
50
40
30
20
10
0
400
600
800
1000
1200
1400
1600
1800
2000
Channel No.
339 KeV(56Ni 339→0)
385.2 KeV(55Fe 1316→931)
411.2 KeV(55Fe411→0)
477.2 KeV(55Fe 1408→1316)
511 KeV
565 KeV (53Cr 565→0)
582 KeV(Na Impurity)
783 KeV(50Cr 783→0)
804 KeV(55Fe 2212→1408)
847 KeV(56Fe 847→0)
931 KeV (55Fe 931→0)
52Cr(α,n)55Fe
Eα = 7 MeV
1275 KeV(Na Impurity)
1316 KeV(55Fe 1316→0)
1408 KeV(55Fe 1408→0)

relative substate populations of the transition. Therefore the coefficients

$$A_k' = \alpha_k A_k \ (J_i, J_f, L, L')$$

where α_k is the ratio of ρ_k to its value in the case of maximum alignment and the $A_k(J_i, J_f, L, L')$ describe the angular distribution of decay radiation in that case, now depending only on level spins and transition multipole orders.

Gamma-ray intensities, also normalized to the 411 KeV peak were also measured. Table I shows these together with the measured angular distribution coefficients, A_2' and A_4'. Recently Sawa (1972) has carried out the $^{52}Cr(\alpha,n)^{55}Fe$ reaction at a bombarding energy of 14.2 MeV and table I includes a comparison with the angular distribution coefficients measured in this experiment. The agreement is excellent, Sawa's results being identical within error in all cases.The spectra were also used to measure branching ratios for the levels in ^{55}Fe by taking ratios of the Legendre polynomial coefficients, A_0, for the states concerned. Figure 4 shows these together with the relevant decay scheme of the low-lying levels of ^{55}Fe. All the branching ratios are those measured in the present work except those from the 2153 KeV state (Robertson et. al. 1970) and the 2050 and 1918 KeV states (Pilt et al. 1970). In general, agreement with other authors is very good.

The angular distribution coefficients were then used to measure gamma-ray mixing ratios δ for several of the transitions. Whenever possible, the mixed transitions were compared directly with pure E_2 decays from the same initial state. A sample calculation is given below for the 931 KeV state. In treating the transition from the 931 KeV $5/2^-$ state to the $3/2^-$ ground state, ratios of A_2' and A_4' for this

Figure 4

Energy levels of ^{55}Fe below 2.5 MeV excitation. Branching ratios are those found in the present work, except those from the 2153 KeV state (Robertson et al. 1970) and the 2050 and 1918 KeV states (Pilt et al. 1970)

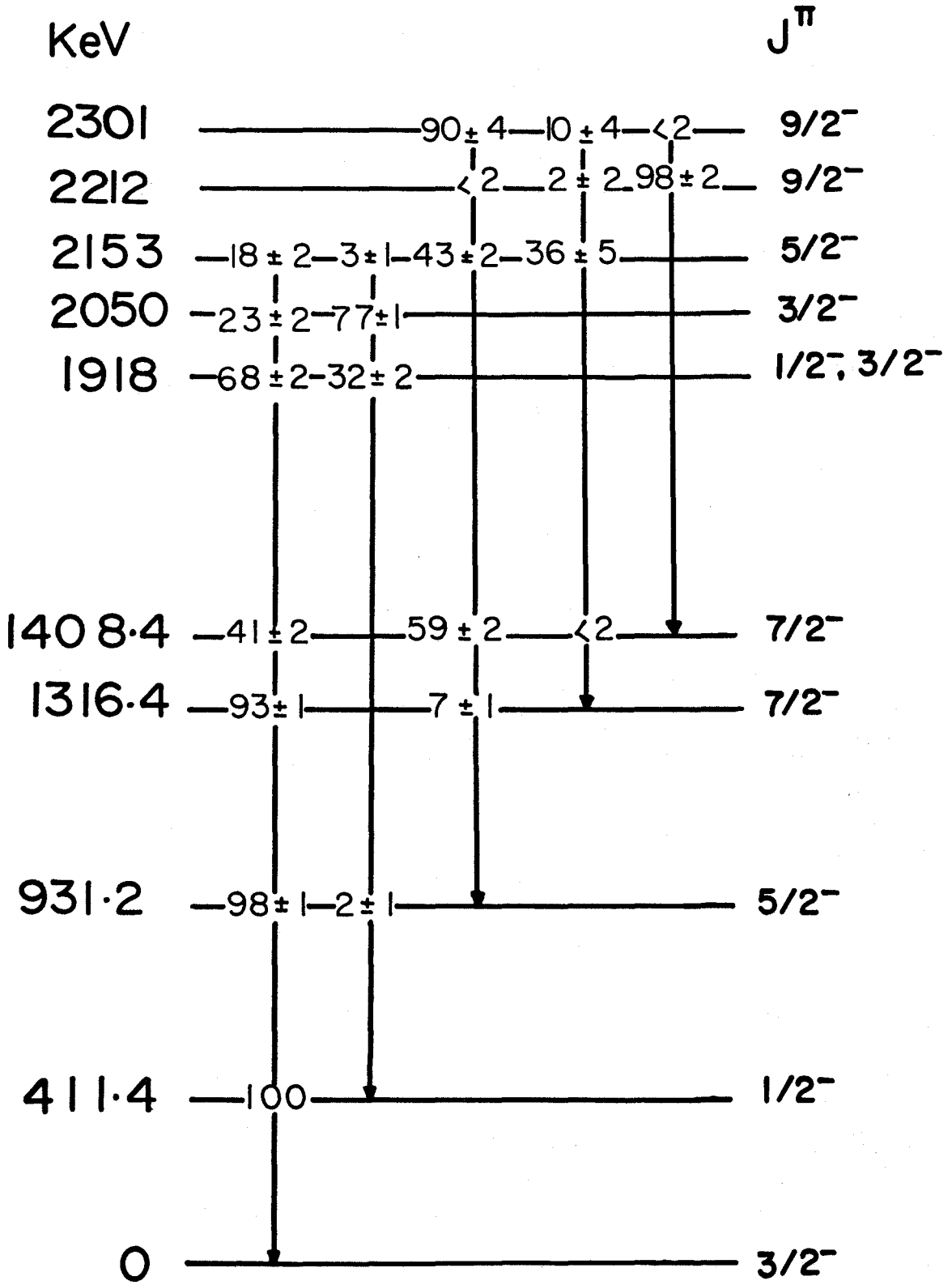
KeV
J^{π}
2301
2212
2153
2050
1918
1408·4
1316·4
931·2
411·4
0
90 ± 4
10 ± 4
< 2
< 2
2 ± 2
98 ± 2
18 ± 2
3 ± 1
43 ± 2
36 ± 5
23 ± 2
77 ± 1
68 ± 2
32 ± 2
41 ± 2
59 ± 2
< 2
93 ± 1
7 ± 1
98 ± 1
2 ± 1
100
9/2⁻
9/2⁻
5/2⁻
3/2⁻
1/2⁻, 3/2⁻
7/2⁻
7/2⁻
5/2⁻
1/2⁻
3/2⁻

TABLE I

Intensities and Angular Distributions of γ-rays from the $^{52}Cr(\alpha,n)^{55}Fe$ Reaction at 7MeV together with a comparison of distributions measured for the same reaction at 14.2 MeV.

				Sawa(1972) -14.2MeV	
Eγ(KeV)	Iγ	A_2'	A_4'	A_2'	A_4'
385	2.6	-0.30(3)	+0.01(5)	-0.298(11)	0.000(17)
411	100	0	0	0	0
477	22	-0.26(1)	-0.01(2)	-0.270(3)	+0.008(4)
520	1.2	+0.38(8)	-0.20(15)		
804	3.4	-0.53(5)	-0.03(9)	-0.577(6)	+0.002(10)
836	11	+0.15(1)	-0.06(2)		
893	1	+0.9 (2)	-0.2 (4)		
896	0.1	+0.1 (2)	-0.5 (3)		
931	83	+0.12(1)	-0.02(1)	+0.123(2)	+0.032(3)
1316	37	+0.36(2)	-0.10(3)	+0.330(6)	-0.063(6)
1408	16	+0.37(3)	-0.06(5)	+0.324(17)	-0.060(18)

transition to those for the pure E_2 decay to the 411 KeV $1/2^-$ level yield the E_2/M_1 mixing ratio of the 931 KeV transition without requiring knowledge of $\rho_k(5/2)$.

Referring to figure 5 and denoting the two relevant gamma rays, 931 KeV→411 KeV (520 KeV) and 931 KeV→ground state (931 KeV), by γ_1 and γ_2 respectively we have, since γ_1 is pure E_2, $A_2^{max}(\gamma_1)$ and $A_4^{max}(\gamma_1)$ are uniquely determined. Here A_2^{max} and A_4^{max} are the values of A_2 and A_4 for complete alignment.

Therefore $A_k^{max}(\gamma_1) = f_k(1/2\ 22\ 5/2) = B_k(5/2)R_k(1/2\ 22\ 5/2)$,

B_k representing the statistical tensor for complete alignment.

Inspection of Yamazaki's tabulation of these coefficients then yields

$$A_2^{max}(\gamma_1) = 0.57143$$

$$\text{and } A_4^{max}(\gamma_1) = -0.57143$$

However, we also have that

$$A_2^{max}(\gamma_2) = \frac{1}{1+\delta^2}\left\{f_2(3/2\ 11\ 5/2)+2\delta f_2(3/2\ 12\ 5/2) + \delta^2 f_2(3/2\ 22\ 5/2)\right\}$$

where δ is the multipole mixing ratio which we want to find. ie.

$$A_2^{max}(\gamma_2) = \frac{1}{1+\delta^2}\left\{-0.400 + 2\delta \times 1.01419 + \delta^2 \times 0.20408\right\}$$

Therefore

$$\frac{A_2^{meas}(\gamma_1)}{A_2^{meas}(\gamma_2)} = \frac{0.57143}{\frac{1}{1+\delta^2}\left\{-0.400+2\delta x1.01419+\delta^2 x0.20408\right\}}$$

Figure 5

Decay of the 931 KeV state in ^{55}Fe

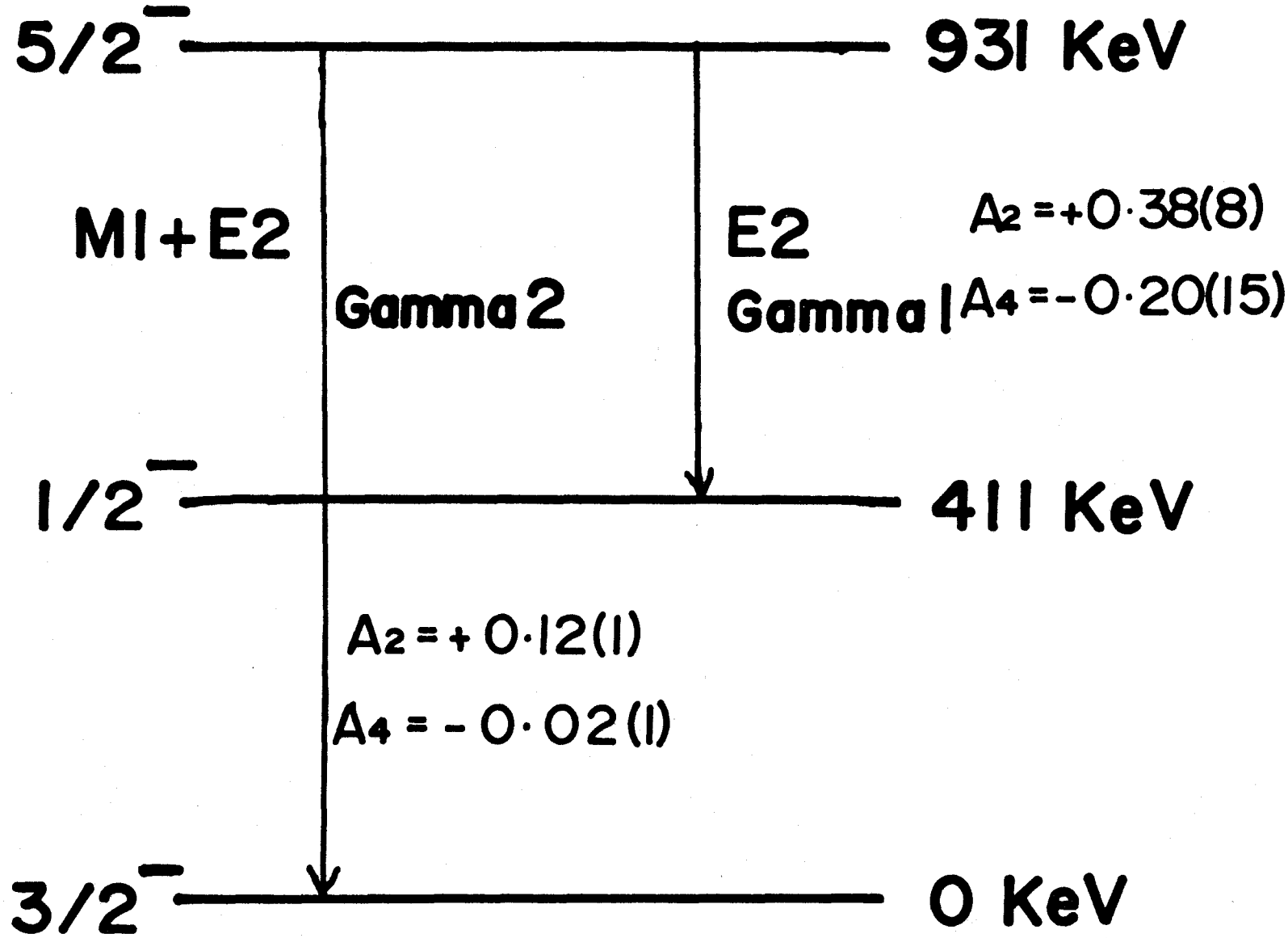
5/2⁻
931 KeV
M1+E2
Gamma 2
E2
Gamma 1
A2 = +0·38(8)
A4 = -0·20(15)
1/2⁻
411 KeV
A2 = + 0·12(1)
A4 = - 0·02(1)
3/2⁻
0 KeV

OR Since $A_2^{meas}(\gamma_1) = A_2^{meas}(520KeV) = +0.38(8)$

and $A_2^{meas}(\gamma_2) = A_2^{meas}(931KeV) = +0.12(1)$

we have

$$\frac{0.38(8)}{0.12(1)} = \frac{0.57143\ (1+\delta^2)}{-0.400 + 2.0284\ \delta + 0.2048\ \delta^2}$$

Solution of this equation gives

$$\delta = 0.29(2) \quad \text{or} \quad |\delta| > 100$$

The A_4 coefficients are now used to give an upper and lower limit on the mixing ratio thus,

$$\frac{A_4^{meas}(\gamma_1)}{A_4^{meas}(\gamma_2)} = \frac{-0.57143}{\frac{\delta^2}{1+\delta^2}\ 0.65306}$$

$$\frac{-0.20(15)}{-0.02(1)} = \frac{-0.57143(1+\delta^2)}{0.65306\ \delta^2}$$

This gives $\delta \sim \pm 0.28$ and hence the value >100 which is possible from solution of the earlier equation may be discarded and δ is therefore equal to 0.29(2).

In general measured mixing ratios were in good agreement with previous work. Table II gives the branching and mixing ratios measured in this experiment together with comparison with the work of previous authors. Values of α_2 are also given in this table. These are as defined earlier in the chapter.

TABLE II

Branching and Mixing Ratios for Transitions in ^{55}Fe up to 2.5 MeV

E_i (KeV)	E_f (Kev)	Branch % This Work	Branch % Others	$E_2\|M_1$ mixing ratios This Work	$E_2\|M_1$ mixing ratios Others	α_2
411	0	100	100			
931	0	98(1)	98(1)	0.29(2)	0.36(1)	0.63 (6)
	411	2(1)	2(1)			
1316	0	93(1)	96(1)			
	931	7(1)	4(1)	-0.03(2)		0.71(5)
1408	0	41(2)	46(2)			
	931	59(2)	54(2)	-0.003(15)		0.73(6)
	1316	<2	<2			
2212	931	<2	<2			
	1316	2(2)	2(1)	0.2(5)		
	1408	98(2)	98(1)			
2301	931	90(4)	92(2)			
	1316	10(4)	8(2)			
	1408	<2	<2			

CHAPTER VI

PERTURBED ANGULAR DISTRIBUTION MEASUREMENTS IN ^{55}Fe

An alloy of 80% iron and 20% chromium was prepared and used as a target for the perturbed angular distribution measurements. The alloy was prepared by melting together the appropriate weights of iron and chromium in a furnace through which a constant stream of inert argon passed. A target of the alloy was made and soldered onto a copper bar, which was held in position in the target chamber by a copper cold finger - see figure 6. The target was water cooled through this cold finger during the course of the experiment. The target is held between the pole tips of an electromagnet, which provides a magnetic field of 3·2 kOe at the centre of the pole-gap when the pole-tips are separated by 5 mm . and a current of 0.8 amps passes through the magnet. Again the target was bombarded with 7 MeV alpha particles.

Ge(Li) detectors of 37 cc and 12 cc volume were fixed at 135^{o} and 225^{o}, as shown, since these are the positions of maximum slopes of the distributions for small A_4. To reduce systematic effects such as fluctuations in pulse height and resolving time, a system has been devised to reverse the field in the electromagnet every 20 secs. (Gibb, 1973). A timer scaler is used in conjunction with a field flip relay circuit, the timer scaler being preset to count 20 second intervals. The system is in turn controlled by a signal to the analyzer of a PDP-9 on-line computer so that should the analyzer be stopped, the field direction will

Figure 6

Schematic diagram of the experimental set up for the perturbed angular distribution measurements

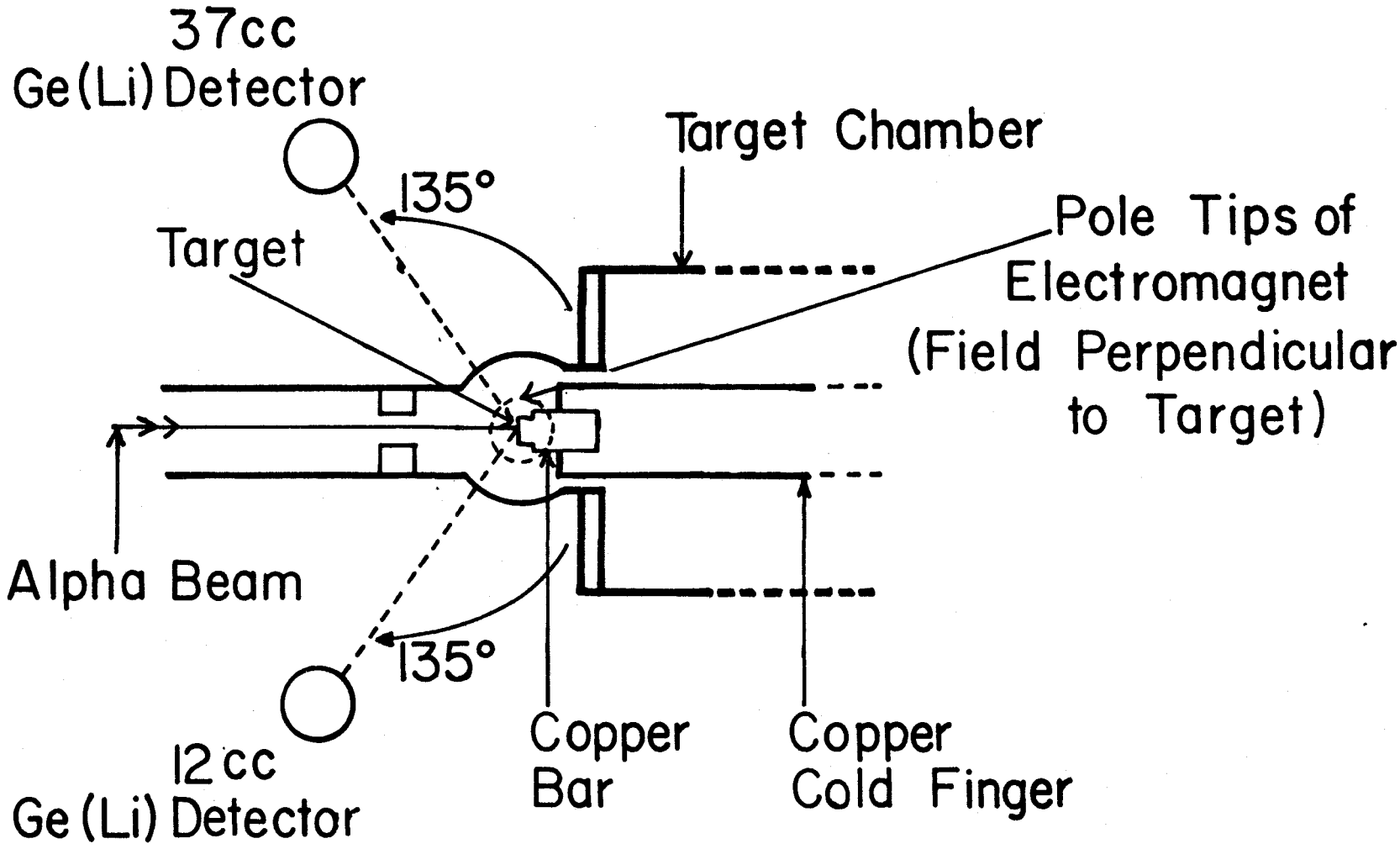
37cc
Ge(Li) Detector
Target Chamber
135°
Target
Pole Tips of
Electromagnet
(Field Perpendicular
to Target)
Alpha Beam
135°
12 cc
Ge (Li) Detector
Copper
Bar
Copper
Cold Finger

not change until it is restarted.

The data were collected in four 2K blocks of memory in the PDP-9 computer, representing X and Y counters with field up and field down respectively. The detectors are connected through Tennelec TC 203 BLR amplifiers to two Nuclear Data analogue to digital convertors. The current passing through the electromagnet is monitored continually to see that it is constant through changes in the field direction. Figure 7 shows a block diagram of the electronics used.

As mentioned in Chapter III, the quantity measured is

$$Q^2 = \frac{W(135^o, +H) \cdot W(225^o, -H)}{W(135^o, -H) \cdot W(225^o, +H)}$$

where +H and -H represent field up and field down respectively.

The spectra were again analyzed off-line on a CDC-6400 computer after having been written on magnetic tape. About 30 hours of counting time were required to obtain reasonable statistics.

The values of Q^2 were now corrected for the effect of the fringing field of the polarizing magnet on the incident ion beam. In addition to displacing the beam spot away from the nominal counter axis, the field alters the angle of incidence of the beam on the target. A consequent change in count-rate due to these effects occurs and it is of course desirable to know whether this involved any considerable correction to the data. Gibb (1973) showed that the ratio of $\frac{Q-1}{Q+1}$ is given by the expression

$$\frac{Q-1}{Q+1} = \frac{\sqrt{2} \cdot \frac{Y}{r} + b_2 \left[\sqrt{2} \frac{Y}{r} - 2\beta \right]}{1-b_4}$$

Figure 7

Block diagram of field switching arrangement and data collection system used in perturbed angular distribution measurements.

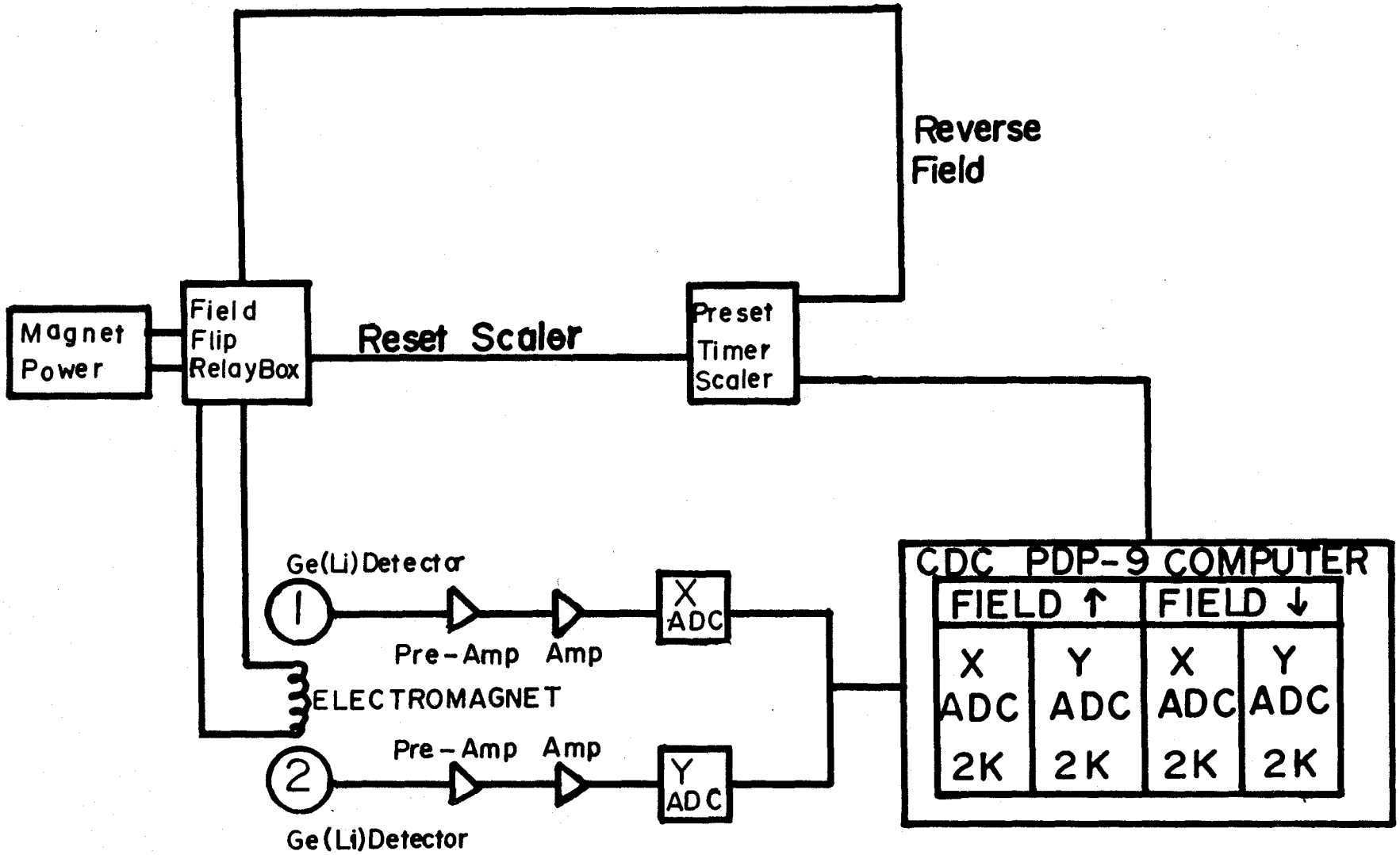
Reverse
Field
Magnet
Power
Field
Flip
RelayBox
Reset Scaler
Preset
Timer
Scaler
Ge(Li) Detector
1
X
ADC
Pre-Amp
Amp
ELECTROMAGNET
Pre-Amp
Amp
2
Y
ADC
Ge(Li) Detector
CDC PDP-9 COMPUTER
FIELD ↑
FIELD ↓
X
ADC
2K
Y
ADC
2K
X
ADC
2K
Y
ADC
2K

where Y is the beam shift and β is the angle through which the beam is rotated. Figure 8 shows the geometry concerned.

Both β and Y can be found by measuring the field distribution of the electromagnet and pole-gap arrangement used in the experiments and carrying out a numerical integration.

With this analysis, Gibb found that the following expression held for calculation of the beam bending,

$$\frac{Q-1}{Q+1} \times 10^3 = (6.39 - 43.9b_2) \frac{Zi}{\sqrt{AE}}$$

where Z = projectile charge state

A = projectile mass number

E = projectile energy

i = magnet current (amperes) .

This expression was used to calculate the beam bending effect for the 411, 477 and 931 KeV γ-transitions in ^{55}Fe for 7MeV alpha particle bombardment. The values for b_2 used where those measured in the earlier angular distribution experiment. The results for $\left(\frac{Q-1}{Q+1}\right) \times 10^3$ are shown in table III and as the formula above suggests a graph of $\left(\frac{Q-1}{Q+1}\right) \times 10^3$ versus b_2 should be a straight line with slope $\sqrt{2}\frac{Y}{r} - 2\beta$ and intercept $\sqrt{2}\frac{Y}{r}$. Figure 9 shows a graph of $\left(\frac{Q-1}{Q+1}\right) \times 10^3$ versus b_2.

The magnitude of the beam-bending correction is seen to depend on the b_2 coefficient. For back angles, the beam shift and beam rotation corrections are opposite in sign for positive b_2 coefficients and add for negative b_2 coefficients.

Figure 8

Beam - bending Geometry

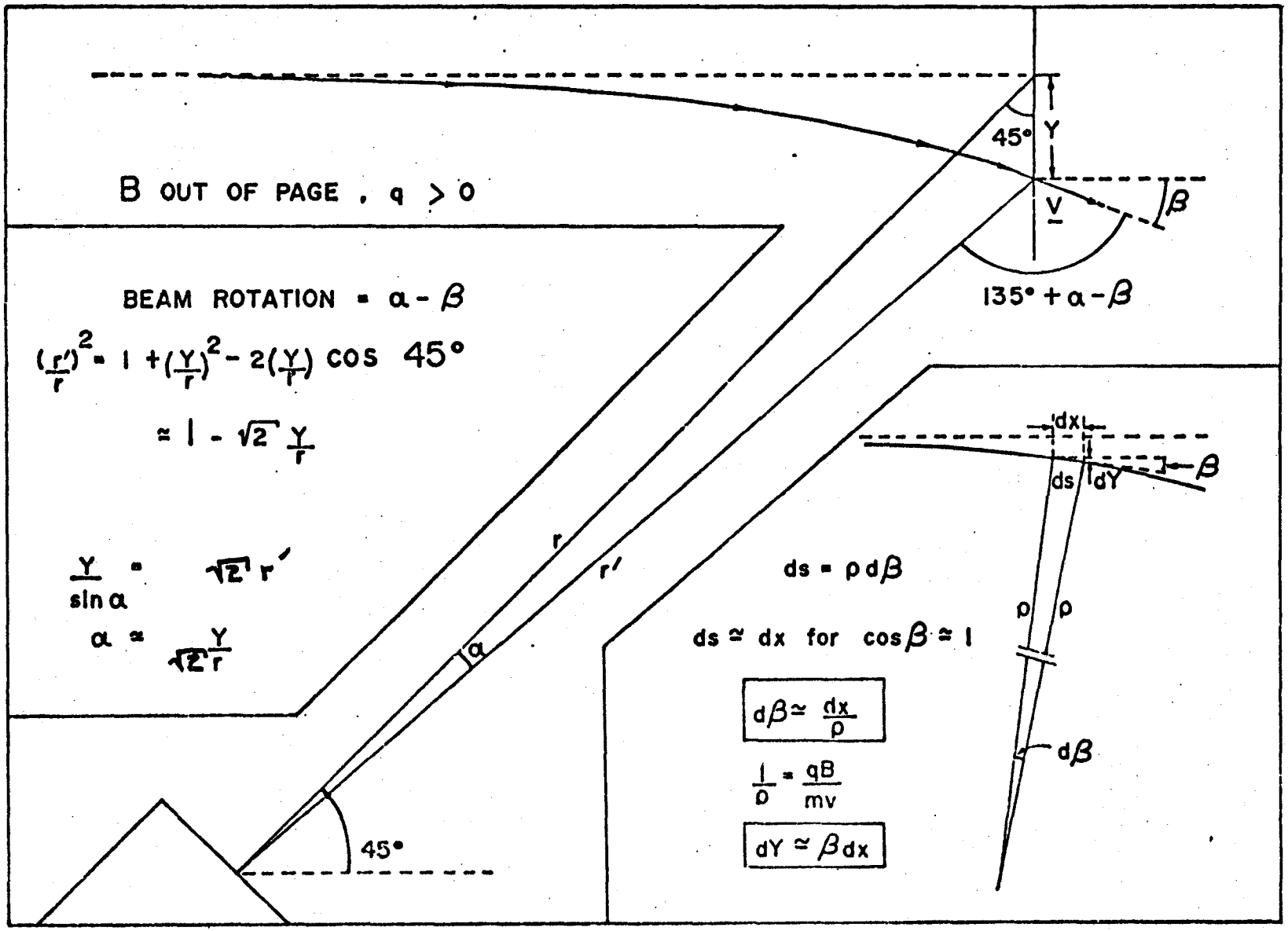
B OUT OF PAGE , q > 0
45°
Y
V
β
135° + α - β
BEAM ROTATION = α - β
$(\frac{r'}{r})^2 = 1 + (\frac{Y}{r})^2 - 2(\frac{Y}{r})\cos 45°$
$\approx 1 - \sqrt{2}\frac{Y}{r}$
$\frac{Y}{\sin\alpha} = \sqrt{2}\,r'$
$\alpha \approx \frac{Y}{\sqrt{2}r}$
r
r'
α
45°
ds = ρ dβ
ds ≃ dx for cos β ≃ 1
$d\beta \simeq \frac{dx}{\rho}$
$\frac{1}{\rho} = \frac{qB}{mv}$
$dY \simeq \beta dx$
dx
ds
dY
β
ρ
ρ
dβ

To give experimental confirmation of the calculated beam bending, a Q^2 measurement was carried out in exactly the same manner as with the alloy target but this time using a pure chromium target. This is of course non-ferromagnetic and any non-zero value measured for $\frac{Q-1}{Q+1}$ must be solely due to beam bending effects. Table III shows also the measured values for Q^2 and $\left(\frac{Q-1}{Q+1}\right) \times 10^3$ for the 411, 477 and 931 KeV transitions and it is seen that there is very good agreement with the calculated values within experimental error. Figure 9 also shows the experimental values of $\left(\frac{Q-1}{Q+1}\right) \times 10^3$ plotted against b_2.

The average rotation angle $\omega\tau$ is related to Q by

$$\frac{Q-1}{Q+1} = \frac{2b_2\ \omega\tau \Big/ \left[1 + (2\omega\tau)^2\right]}{1 - b_4 \Big/ \left[1 + (4\omega\tau)^2\right]}$$

and hence the rotation angles corresponding to the measured Q^2 values could be determined. Table IV shows the Q^2 values corrected for beam bending together with the coefficients b_2 and b_4 and $\omega\tau$ for the states in ^{55}Fe at 931, 1316 and 1408 KeV (from measurement of the 477 KeV state) and also the 847 KeV first excited state in ^{56}Fe which is present in the spectrum due to the iron present in the target.

TABLE III

Calculated and experimental values of $\left(\frac{Q-1}{Q+1}\right) \times 10^3$ for states in ^{55}Fe for beam bending estimations in a pure Cr target

		Experimental		Theoretical
$E\gamma$ (KeV)	b_2	Q^2	$\left(\frac{Q-1}{Q+1}\right) \times 10^3$	$\left(\frac{Q-1}{Q+1}\right) \times 10^3$
411	0	1.0064(8)	1.59(25)	1.93(10)
477	-0.208(11)	1.0203(16)	5.02(40)	4.69(24)
931	+0.080(5)	1.0028(9)	0.69(19)	0.87(5)

Figure 9

Comparison of experimental and theoretical values of $\left(\frac{Q-1}{Q+1}\right) \times 10^3$ versus b_2 for the $^{52}Cr(\alpha,n)^{55}Fe$ reaction at 7MeV

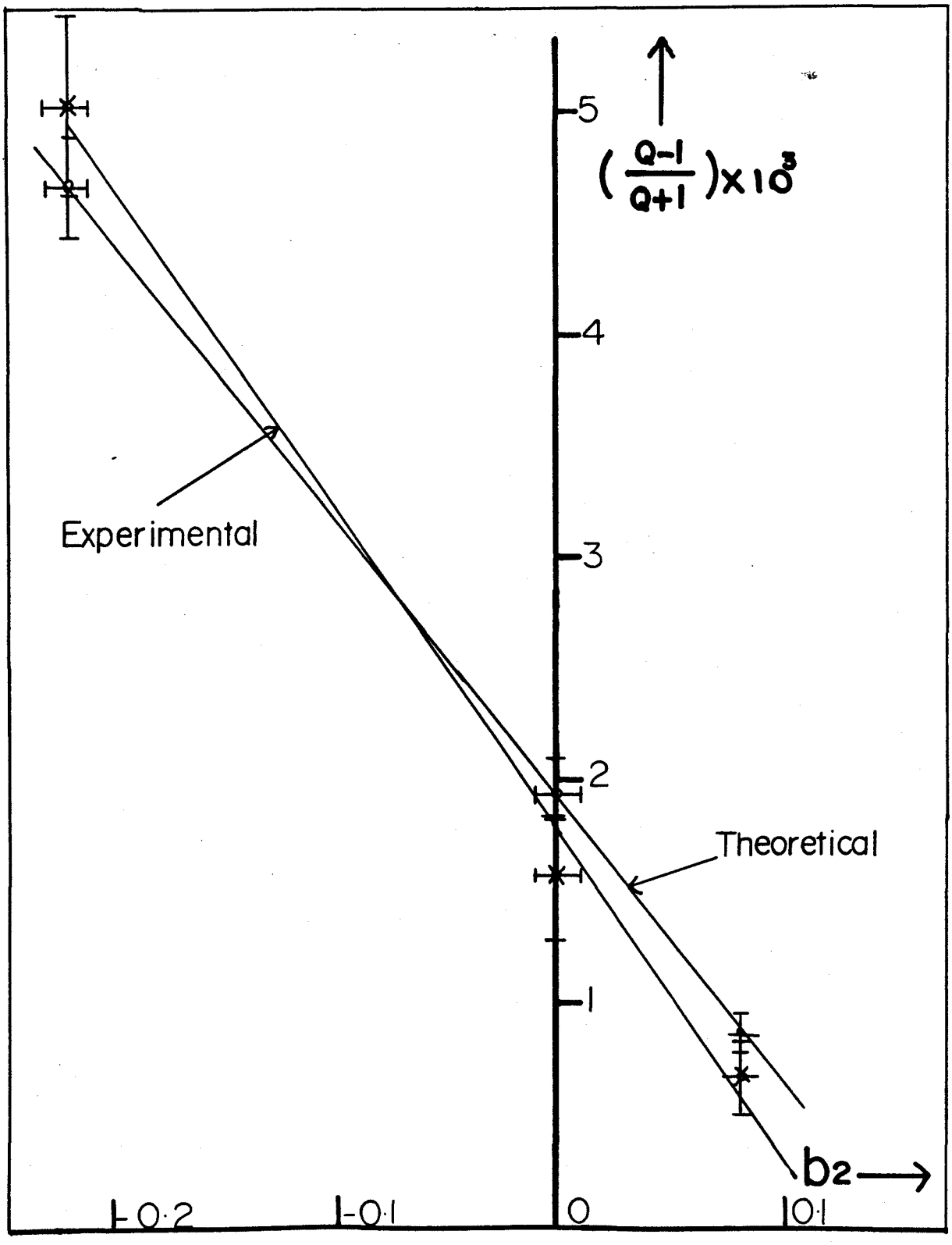
5
4
3
2
1
$(\frac{Q-1}{Q+1})\times 10^3$
Experimental
Theoretical
b_2
-0·2
-0·1
0
0·1

TABLE IV

PERTURBED ANGULAR DISTRIBUTION MEASUREMENTS IN ^{55}Fe

Level (KeV)	Eγ (KeV)	Q^2	b_2	b_4	ωτ (milliradians)
847 (^{56}Fe)	847	1.015(2)	+0.265(4)	+0.058(5)	6.5(9)
931	931	1.011(2)	+0.080(5)	-0.010(5)	17(3)
1316	1316	1.001(1)	+0.222(11)	-0.053(13)	0.6(6)
1408	477	1.088(3)	-0.208(11)	-0.005(10)	-50(3)

CHAPTER VII

MEASUREMENT OF THE HYPERFINE FIELD IN THE ALLOY $Fe_{80}Cr_{20}$

The final part of the experimental work in this project consisted in measuring the hyperfine field present in the alloy used in the experiment, $Fe_{80}Cr_{20}$. To extract g-factors from the measured rotation angles, values for the static and transient fields must be known. The recoil energy of ^{55}Fe ions following the (α,n) reaction on ^{52}Cr at 7MeV is only $\sim$ 0.5 MeV and hence the transient rotation is unlikely to exceed a few milliradians. Confirmation of this expectation was found in the measured rotation for the ^{56}Fe 2+ level at 847 KeV - table IV. The value, 6.5(9) milliradians is consistent with the value measured previously in resonance fluorescence and radioactive decay measurements in pure iron (Metzger, 1961, Appel and Mayer, 1963) and in low energy (P,P') excitation (Kalish and Kossler, 1968). The reduction from their value of 8 milliradians was exactly in proportion to the reduction in the static field value measured in this work.

The measurement of the static field consisted of the measurement of the Mössbauer absorption spectrum of ^{57}Fe in the target sample. This was done by powdering a specimen of the alloy used for the target and measuring its absorption spectrum with the Mössbauer apparatus available in the McMaster Chemistry Department (T. Birchall, 1972). As a calibration of the spectrum, the Mossbauer spectrum of an iron foil enriched in ^{57}Fe was measured. As indicated in Chapter IV, the spectrum of

pure ^{57}Fe consists of six peaks and the centroids of these peaks will be shifted in the spectrum of the target alloy due to the change in hyperfine field. The spectra obtained are shown in figure 10. The spectrum from the target sample represents about 24 hours in counting time. The measured centroid positions of the peaks indicated an average field of 277 kOe, compared with the known value of 333 kOe in pure Fe. The standard deviation of the field distribution, as reflected in the broadening of the lines, was 15%, or half the field reduction, as would be expected for a binomial distribution of Cr atoms at the 16 or so neighbour sites which are responsible for most of the deviation.

The contributions to the internal field at Fe nuclei in Fe Cr alloys for low concentration alloys have been analyzed by several workers. Recent work has been carried out by Cranshaw (1971) who measured Mössbauer absorption spectra for alloys with up to 4.8% Cr. He gave the individual deviations in the Fe field caused by the replacement in each shell of neighbours of single Fe by Cr atoms. Assuming random population of these shells by Fe and Cr atoms in the ratio 4:1 in the alloy used in these experiments, and further assuming additivity of the deviations to this high concentration, one arrives at a value for the reduction in the average field at the Fe nuclei of 25%. On the other hand, the addition of Cr atoms to iron appears to increase the average spin density somewhat. This would increase the field by 8% for a 20% alloy giving a final field of about 275 kOe. This is of course in excellent agreement with the value measured in this experiment.

In the following g-factor calculations therefore, the hyperfine field in the alloy $Fe_{80}Cr_{20}$ was taken to be

Figure 10

Mössbauer absorption spectrum of ^{57}Fe in

(a) a powdered specimen of $Fe_{80}Cr_{20}$ alloy and

(b) in pure iron foil enriched with ^{57}Fe

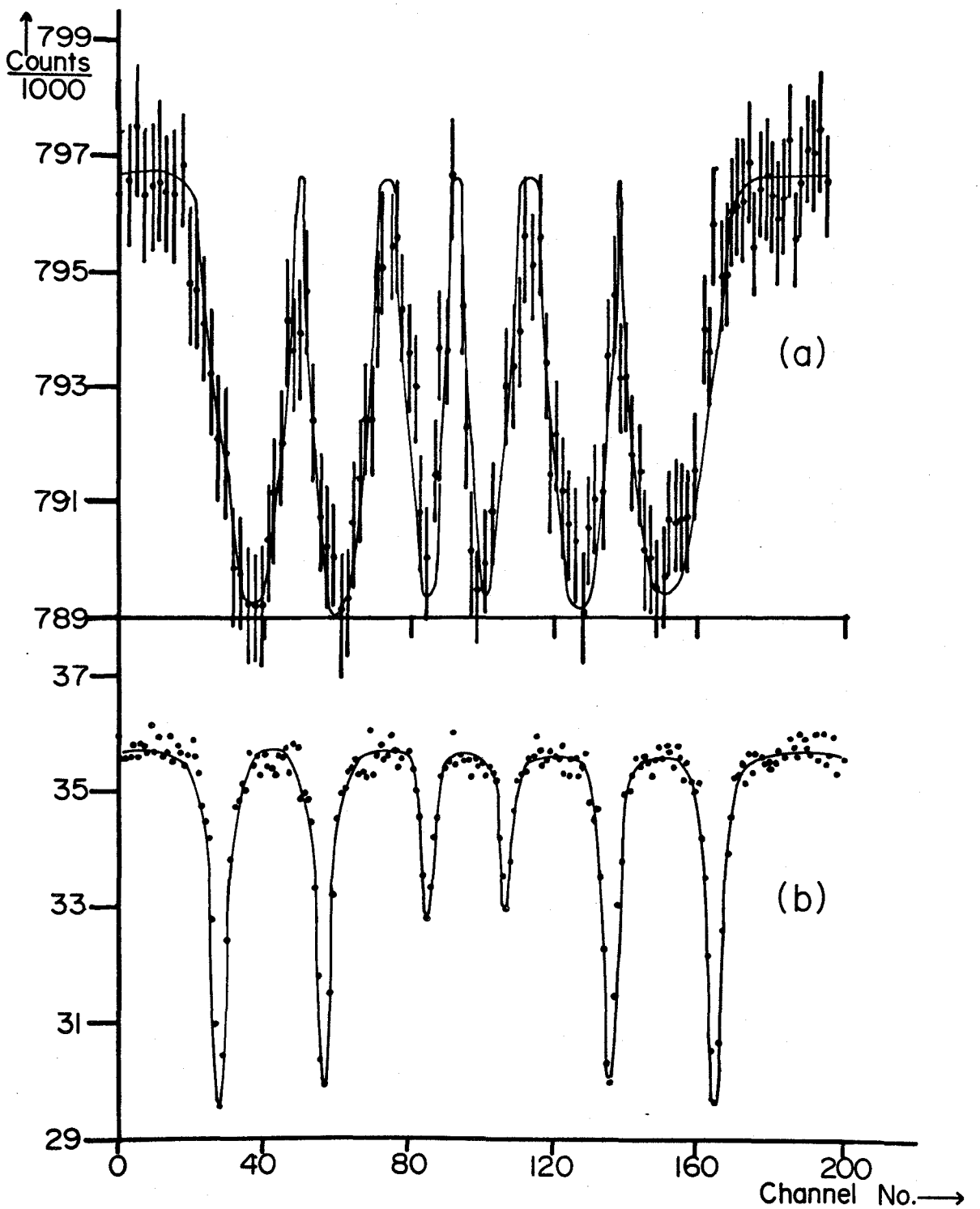
799
Counts
1000
797
795
793
791
789
37
35
33
31
29
(a)
(b)
0
40
80
120
160
200
Channel No.⟶

$$|H_{hyp}| = 277\ (\pm 6)\ \text{kOe}$$

This Mössbauer measurement cannot in itself give the sign of the field but, as mentioned in Chapter VI, along with the measurements of the rotations of states in ^{55}Fe, the rotation of the 847 KeV 1st excited state in ^{56}Fe was also measured. This rotation was found to have a negative sign. Since the sign of the g-factor of this state is known to be positive, this implies that the sign of the field is itself negative.

ie. $H_{hyp} = -277\ (\pm 6)\ \text{kOe}$

CHAPTER VIII

RESULTS AND DISCUSSION

As pointed out earlier, the rotation angle $\omega\tau$, the field H, and the lifetime τ are related by the equation

$$\omega\tau = \frac{g\mu_N H\tau}{\hbar}$$

where μ_N is the nuclear magneton and g is the nuclear g-factor.

It remains therefore necessary only to know the lifetimes of the states under study and the nuclear g-factors may then be obtained. It is a general trend that measurements of nuclear lifetimes at present tend to involve rather large experimental error and although the lifetimes of the low-lying levels in ^{55}Fe have been measured in recent years, the above is true here and the greatest error in the final g-factor measurements is due to these uncertainties in the lifetimes of the states. Lifetime measurements in ^{55}Fe have been reported by Robertson (1970, 1972) in two separate papers, the earlier work involving lifetime measurements by the Doppler Shift Attenuation Method (DSAM) and the later work using this method as well as direct timing. Donahue and Hershberger (1971) have also reported lifetime measurements in ^{55}Fe using the DSAM method. Table V shows the lifetimes measured by these authors.

Robertson has not measured the lifetime of the 931 KeV state so the lifetime used here was necessarily that of Donahue and Hershberger.

TABLE V

LIFETIMES IN ^{55}Fe (in units of fs.)

Level (Kev)	1970 DSAM(solid)	Robertson 1972 DSAM	1972 direct timing	Donahue + Hershberger DSAM (gas)
931				$11(4) \times 10^3$
1316	910^{+910}_{-310}	950^{+3050}_{-410}	$< 10 \times 10^3$	$(14 \pm 3) \times 10^3$
1408	>840	>950	$(49 \pm 10) \times 10^3$	$(40 \pm 20) \times 10^3$

For the 1408 KeV state the direct timing measurement of Robertson was used, this being in good agreement with Donahue and Hershberger's less precise value for this state. The obvious discrepancy in these measurements is in the lifetime of the 1316 KeV state. The value chosen was 910 $^{+910}_{-310}$ ps. as measured by Robertson and this results in the g-factor of the 1316 KeV state being +0.5(5). However, consideration should be taken to see how this value is altered by a choice of Donahue and Hershberger's lifetime measurement - (14±3) x 10^3 ps. This suggests a value for g of 0.03(3). This is within the error for the g-factor estimated using Robertson's value and so the discrepency between these lifetimes is not too important in the present measurement.

Using these lifetimes, the g-factors measured for the states at 931, 1316, and 1408 KeV are shown in Table VI.

Now to a first approximation, the magnetic moment of a nucleus may be taken to be the vector sum of the individual nucleons, ie. The magnetic moment is usually assumed to be a sum of single particle operators of the form

$$\mu = \sum_i g_l \, l_i + g_s \, s_i$$

with $g_l = 1,0$; $g_s = 5.58, -3.82$ for the proton and neutron respectively. Certain deviations occur from this formula (Bodenstedt and Rogers (1964) due to quenching of the anomalous magnetic moment when nucleons are in nuclei, meson exchange currents, relativistic mass changes for nucleons in nuclei, and velocity dependent potentials in the nucleus, but such deviations are small (~0.2 nuclear magnetons). Another factor which influences agreement between theory and experiment is the lack of knowledge of the correct form of the nuclear wave functions. These wave

TABLE VI

g-FACTORS IN ^{55}Fe

Level (KeV)	Jπ	ωτ (mrad)	τ (ps)	g	g Schmidt
931	$5/2^-$	17(3)	11(4)	+1.2(5)	+0.55
1316	$7/2^-$	0.6(6)	$0.9^{+.9}_{-.4}$	+0.5(5)	-0.55
1408	$7/2^-$	-50(3)	49(10)	-0.77(16)	-0.55

functions are derived from nuclear models, the basis of the microscopic model being the shell model (Mayer 1949). Since ^{55}Fe can be described as a single neutron outside and two proton holes in the double closed f 7/2 shell, it may be treated simply within the shell model formulation (Ohnuma, 1966, Vervier, 1966). Of these the calculations of Ohnuma have been the most successful in reproducing most of the known structure.

In the shell model nucleons are assumed to pair off, the paired nucleons giving no contribution to the magnetic moment. In this formalism, the so-called Schmidt limits for the magnetic moments for the odd-A nuclei are given by the formula

$$\mu = j \left(g_l \pm (g_s - g_l) \frac{1}{2J+1}\right)$$

with $j = l \pm s$

For the majority of nuclei the measured magnetic moments tend to lie within the Schmidt limits. Such deviations are assumed due to the inadequacy of the shell-model wave functions. In Table VI a comparison with the Schmidt limits for the states concerned is shown.

Clearly the g-factor measured for the 1408 KeV state, which is thought to be a neutron hole lies extremely close to the g-factor calculated for a pure f 7/2 neutron, clearly confirming the hole nature of this state.

To explain the g-factors measured for the states at 931 KeV and 1316 KeV one must consider admixtures of other single particle states through the core excitations. Such a model is called the intermediate coupling model and ^{55}Fe has been treated recently in this formalism by Carola et al. (1970) and Csürös et al. (1971). In the

intermediate coupling model the odd nucleon is coupled to the neighbouring even core, which is either in its ground state or an excited state. The core is considered to be capable of performing quadrupole oscillations. The major discrepency in the calculation of the level scheme for ^{55}Fe is that the model does not take account of the $7/2^-$ and $9/2^-$ levels at 1408 KeV and 2212 KeV, which are both thought to arise from a creation of a hole in the f $7/2$ shell.

The g-factors for the two $7/2^-$ states measured here appear to differ. It would appear that the 1316 KeV state is strongly admixed with states with g>0 Likely admixtures are the f $5/2$ neutron state and, of course, the 2+ state of the ^{54}Fe core, which has recently been shown to have a g-factor near to that of an f $7/2$ proton (Hubler et al. (1972).

Figure 11 compares the g-factors measured for the two $7/2^-$ states with those previously measured for $7/2^-$ states in other odd-neutron nuclei.

To conclude then, this work has confirmed previous measured electromagnetic properties of the ^{55}Fe nucleus and has utilized the method of perturbed angular correlations to establish g-factors, previously unknown, for three of the low-lying states.

Figure 11

Nuclear g-factors of $7/2^-$ states of odd neutron nuclei.

The dashed line is the Schmidt limit for f 7/2.

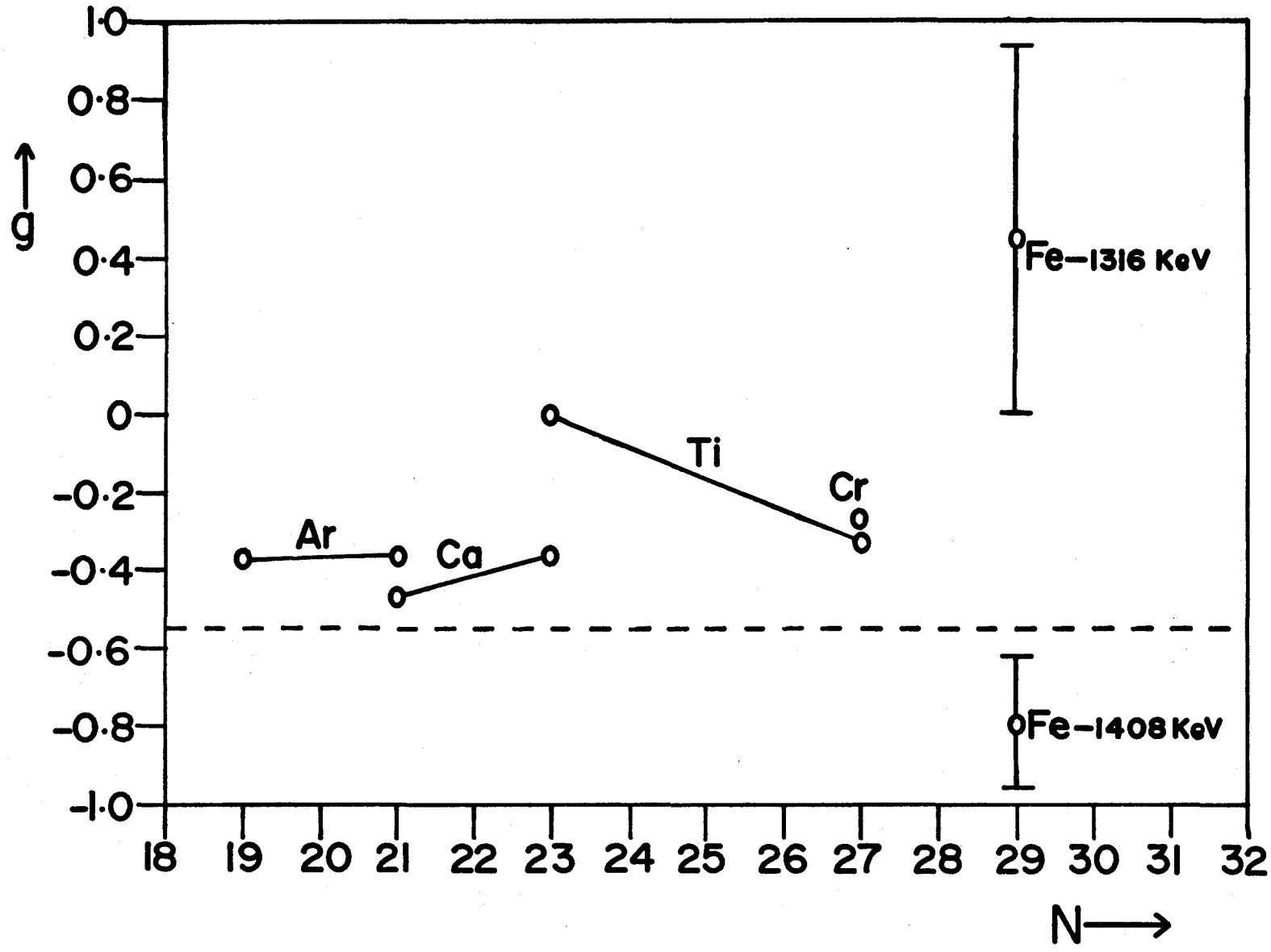
1·0
0·8
0·6
0·4
0·2
0
-0·2
-0·4
-0·6
-0·8
-1·0
g
18
19
20
21
22
23
24
25
26
27
28
29
30
31
32
N
Ar
Ca
Ti
Cr
Fe–1316 KeV
Fe–1408 KeV

BIBLIOGRAPHY

Aeppli, H., Bishop, A.S., Frauenfelder, H., Walter, M. and Zunti, W., 1951, Phys. Rev. 82 550

Appel, H. and Mayer, W., 1963, Nucl. Phys. 43, 393

Birchall, T., 1972, Private Communication

Bodenstedt, E. and Rogers, J.D., 1964 in Perturbed Angular Correlations, pp. 93-151 Edited by Karlsson, E., Matthias, E. and Seigbahn, K., (North-Holland Publishing Co., Amsterdam).

Carola, T.P.G. and Ohnuma, H., 1971, Nucl. Phys. A165, 259

Cranshaw, T.E., 1972, J. Phys. F. Metal Physics, 2, 615

Csürös, M., Cameron, J.A. and Zámori, Z., 1971, Can. J. Phys. 49, 1832

Donahue, D.J. and Hershberger, R.L., 1971 Phys. Rev. C4, 1693

Frauenfelder, H., Lawson, J.S., and Jentschke, W., 1954, Phys. Rev. 93, 1126

Frauenfelder, H., and Steffen, R.M., Alpha-Beta-and Gamma-Ray Spectroscopy 1965, pp. 997-1198. Edited by Seigbahn, K., (North-Holland Publishing Co., Amsterdam).

Ferguson, A.J., 1965, Angular Correlation Methods in Gamma-Ray Spectroscopy, (North-Holland Publishing Co., Amsterdam).

Gibb, A.W., 1973, Ph.D. Thesis, McMaster University

Hubler, G.K., Kugel, H.W., and Murnick, D.E., 1972, Phys. Rev. Letters 29, No. 10, 662

Kalish, R. and Kossler, W.J., 1968, Phys. Rev. Letters, 20, 271

Marshall, W., 1958, Phys. Rev. 110, 1280

Mayer, M.G., 1949, Phys. Rev., 75, 1969

Metzger, F.R., 1961, Nucl. Phys. 27, 612

Mössbauer, R.L., Z. Physik, 1958, 151, 124

----------. Z. Naturforsch, 1959 149, 211

Ohnuma, H., 1966, Nucl. Phys., 88, 273

Pilt, A.A., Sheppard, D.M., Olsen, W.C., Carola, T.P.G. and Twin, P.J., 1970, Nucl. Phys., A150, 439

Robertson, B.C., Carola, T.P.G., Sheppard, D.M. and Olsen, W.C., 1970, Nucl. Phys., A160, 137

Robertson, B.C., Neilson, G.C. and McDonald, W.J., 1972, Nucl. Phys., A189, 439

Rose, H.J. and Brink, D.M., 1967, Rev. Mod. Phys., 39, 306

Sawa, Z., 1972, Physica Scripta, 6, 11

Shirley, D.A. and Westenbarger, G.A., 1965, Phys. Rev., 138, (1A), 170

Vervier, J., 1966, Nucl. Phys., 78, 497

Watson, R.E. and Freeman, A.J., 1961, Phys. Rev., 123, 2027

Yamazaki, T., 1967, Nuclear Data Sheets, Section A, Vol. 3, No. 1, 1